Supplementary Appendix

This appendix has been provided by the authors to give readers additional information about their work.

Supplement to: Suthana N, Haneef Z, Stern J, et al. Memory enhancement and deep-brain stimulation of the entorhinal area. N Engl J Med 2012;366:502-10.

Supplementary Appendix

Table of Contents

METHODS

N.S., B.K., and I.F. designed the study, wrote the paper and decided to publish the paper. N.S. wrote the first draft of the paper. N.S., Z.H., and J.S. gathered the data and N.S., R.M., and E.B. analyzed the data. All authors vouch for the data and the analysis. There were no confidentiality agreements between the authors and the sponsors of the research.

Behavioral Tasks. In order to familiarize subjects with the tasks, alternate versions (with different stimuli) were given prior to testing. During each spatial learning block, subjects actively explored a virtual environment using a joystick (Figure 1) by searching for passengers and delivering them to designated locations (i.e. stores). For all navigation trials, passengers were positioned in the center of a rectangular grid-like city (Figure 2A). Starting point of each trial began from the previous trial's store location and therefore varied on each trial. Subjects were not told when stimulation was applied.

For the study, we used two different cities (city A and B). Each city used different stores and

locations. The first trial of half of the City A and B sessions started with stimulation and alternated every trial. Therefore stimulation was equally likely to occur during navigation to each store within each city across the six sessions. For the entorhinal stimulation sessions we used city A for four sessions and city B for two sessions. For the hippocampus stimulation sessions we used City A for two sessions and B for four of the sessions. Similar to the entorhinal stimulation sessions, all hippocampal stimulation occurred equally often during navigation to each store. Different locations were used for stimulation and nonstimulation conditions for each subject, with each location equally likely to be learned under stimulation or nonstimulation conditions across subjects.

Four of the seven subjects had electrodes present in both the entorhinal area and the ipsilateral hippocampus. These subjects completed the task for both stimulation sites, using different cities (City A and B) for each session. At least 20 min intervened between hippocampal and entorhinal sessions, and the order of which stimulation site was tested first was counterbalanced across subjects. Specifically, the four of seven subjects who completed both the hippocampus and entorhinal sessions were subjects 2, 3, 4 and 7. Two of these four subjects (subjects 2 and 3) completed the hippocampus component first and two (subjects 4 and 7) completed the entorhinal component first. One of the subjects (subject 5) with bilateral hippocampal electrodes completed one session with right hippocampal stimulation and one with left hippocampal stimulation; different cities (city A and B) were used for these two different sessions.

Two control tasks were interspersed within the spatial learning blocks. The first task was a guided navigation task in which, subjects were instructed to follow the arrows (left or right) on a screen using the joystick (Figure 2C); each block lasted 1 min with stimulation during either the first or last 30 seconds of the task (whether stimulation occurred first was counterbalanced across subjects). During the 30-sec stimulation periods, stimulation was given in 5-sec on/off trains with stimulation parameters identical to those used during the spatial navigation blocks. The second control task was a store-matching task where subjects had to press the corresponding button in order to select one store that matched the target store presented above

(Figure 2B). Block durations were also 1 min and each trial was present for 4 seconds with a 1 sec inter-trial interval.

All stimuli were presented using a Macintosh laptop computer. PyEPL (Python Experiment Program Library; http://pyepl.sourceforge.net/) was used to present virtual reality stimuli and to record navigational routes and key press reaction times. Excess path length, latency, and reaction time performance on the control tasks was calculated using Matlab (Mathworks, Inc).

***Electrode Localization*.** High in-plane resolution structural images with a matrix size of 512 x 512 (spin echo, TR = 5200 ms, TE = 105 ms, 19 slices, contiguous; voxel size: 0.391 x 0.391 x 3 mm) were acquired in the oblique coronal plane perpendicular to the long axis of the hippocampus. Subjects also received a 3-T whole brain T1 weighted MP-RAGE GRE scan (TR = 1800 msec, TE = 2.93 sec, voxel size = .9 x .9 x .8mm) as part of depth-placement planning. Subjects were then implanted with depth-electrodes by stereotactic methods for seizure monitoring as previously described (Fried et al., 1999). Following implantation with depth-electrodes, subjects received a Spiral computed tomography (CT) scan (1 sec rotation, high-quality (HQ) mode, helical pitch 1.5, 1 mm slice collimation, and a 0.5 mm reconstruction interval to localize electrodes). CTs were registered to the high-resolution MRI and to the whole brain MRI using a 3-way registration in BrainLab stereotactic and localization software (www.brainlab.com; Gumprecht et al., 1999; Schlaier et al., 2004). Electrode contacts were registered and visualized on the high-resolution coronal MRI (Figure 1). MTL subregions were anatomically determined by boundaries that were demarcated based on atlases correlating MRI visible landmarks with underlying cellular histology (Amaral and Insausti, 1990; Duvernoy, 1998). These methods have previously been used to localize microelectrodes and investigate structural and functional dissociations within human MTL subregions (Suthana et al., 2009; Ekstrom et al. 2008, Zeineh et al., 2003).

Localization of stimulating electrodes to subjects' high-resolution MRI suggest placement within the human perforant pathway in agreement with recent high-resolution diffusion tensor imaging (DTI) studies in humans (Augustinack et al., 2010; Yassa et al., 2010).

Electrophysiological Recordings and Analysis. For each patient, the threshold for eliciting an after-discharge was determined immediately prior to behavioral testing. The presence of after-discharges was determined by a clinical neurologist (Z.H or J.S). The stimulation current level for the study was set 20-25 percent below the after-discharge threshold determined for each patient. For all subjects, no seizures occurred the day of testing. Each data record was individually examined for after-discharges, artifacts and noise before being included in the EEG analysis (< 2 % of stimulation epochs eliminated).

EEG data were analyzed with Matlab (Mathworks, Inc). We compared the power of the averaged waveforms (theta-phase resetting) for the stimulation and nonstimulation trials for each subject (Figure 4B). For stimulation trials, we compared the averaged waveforms for the 5-second period immediately after the start of the stimulation navigation trial to the 5-second period immediately before the start of the trial. For nonstimulation trials, we obtained comparable averaged waveforms by averaging the waveforms for comparable 5-second periods after and before the trial onset for nonstimulation learning trials (Figure 4B). Also, to ensure that theta-phase resetting was not due to increases in the power of each trial's rhythm, we also calculated the power of each trial during the 5-second period after trial onset across all stimulation and nonstimulation navigation trials (Figure 4C). We also repeated the phase-resetting and power analyses for each of the four frequency ranges (theta, alpha, beta, and gamma).

RESULTS

Quantification of theta-phase resetting across all four subjects yielded a significant increase in power of the final average waveform (i.e. theta-phase resetting) during stimulation vs. nonstimulation trials (Figure 4B; N=4; stimulation > nonstimulation, $t_{(3)} = 5.39$; $p = 0.018$).

Figure 4A shows and example subjects' hippocampal theta-phase resetting (shown visually as an increase in power of the averaged waveform) after stimulation of the entorhinal region. Shown is the final average waveform from one subject of all stimulation and nonstimulation navigation trials during 5 sec pre-trial and during the 5 sec post-trial onset periods.

Hippocampal theta-phase resetting was not due to individual trial differences in theta power (Figure 4C); average theta power of individual waveforms during stimulation vs. during nonstimulation trials was not significantly different. This suggests that stimulation did not merely evoke a larger theta rhythm, but rather phase-shifted an ongoing theta rhythm. We did not find significant changes during stimulation in either phase resetting (power of the average waveforms) or average power in all other frequency ranges (alpha, beta, and gamma).

Example of a store stimulus

Figure 1. An example store stimulus which subjects were instructed to locate in a virtual environment using a joystick controller.

Experimental design

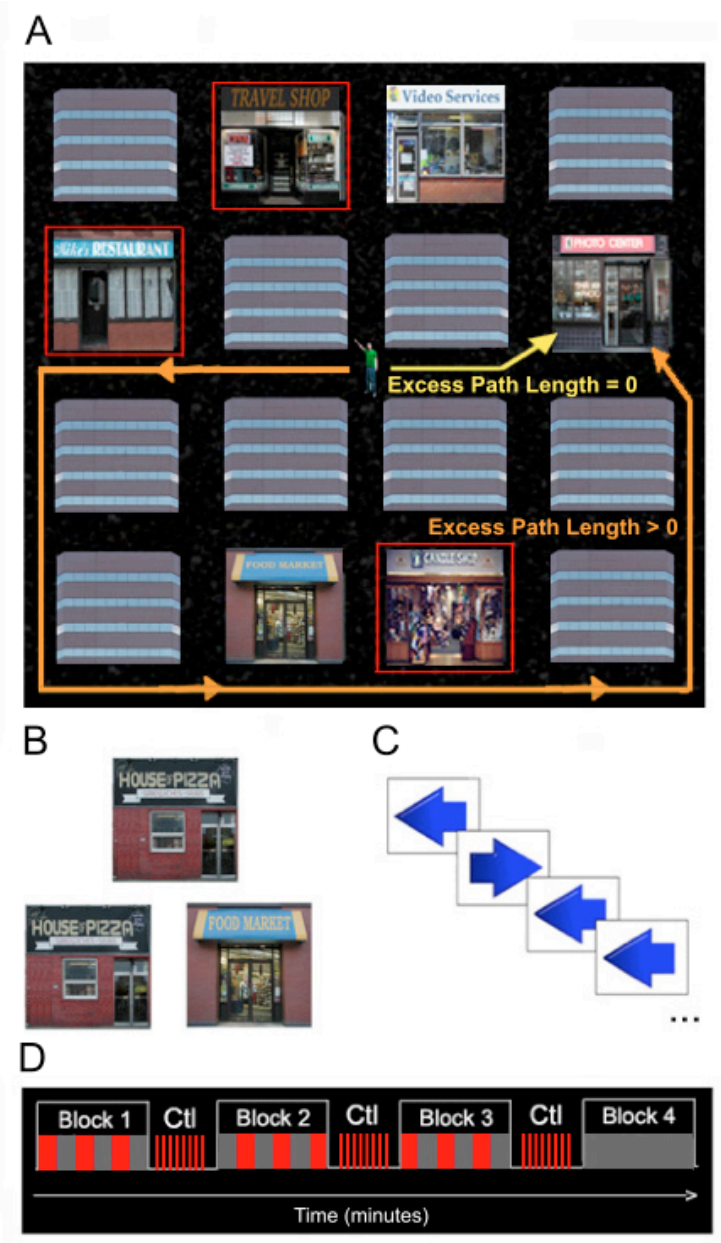

Figure 2. (A) Top down view of an example virtual city that was used showing stores and buildings. Arrows show behavioral measurement of excess path length. Shorter excess path length (yellow) equals better performance. Red outlined stores show example stores in which stimulation is turned on during navigation. (B) Stimuli presented during store-matching task and (C) direction-pressing control tasks. (D) Experimental paradigm consisted of alternating blocks of navigation and control (Ctl) tasks. Red shows stimulated trials. During block 4 (retention) no stimulation is given on any trial.

Behavioral performance on control tasks

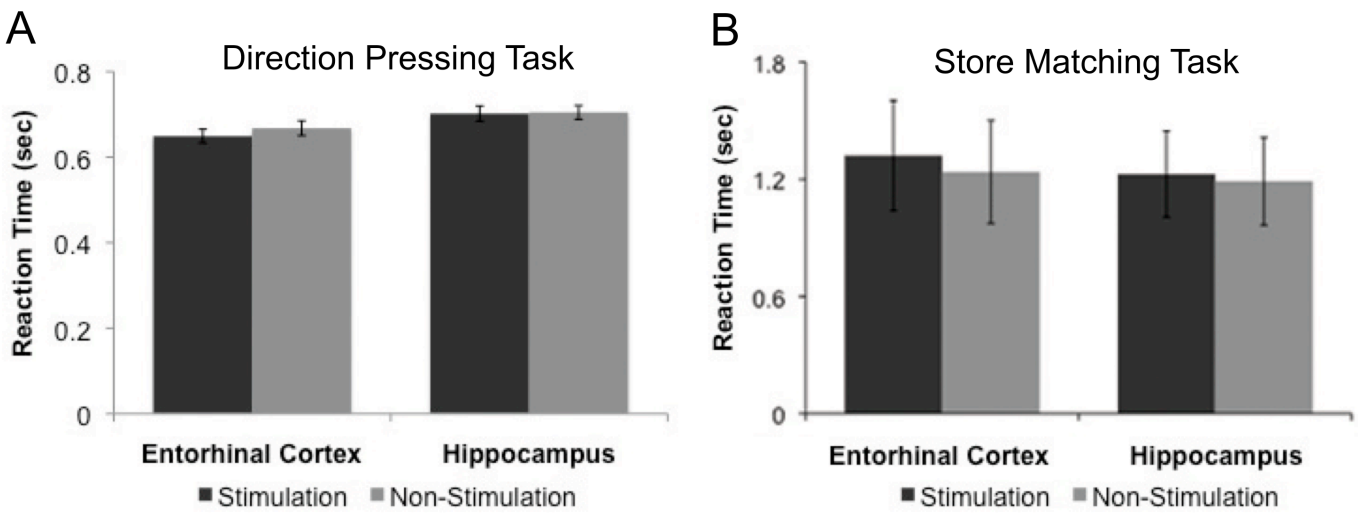

Figure 3. Reaction time during the (A) direction-pressing and (B) store-matching control tasks with and without stimulation of entorhinal (N = 6) and hippocampal (N = 6) regions. No significant differences in reaction time were found. Error bars correspond to the standard error across subjects for each condition.

Hippocampal theta-phase resetting

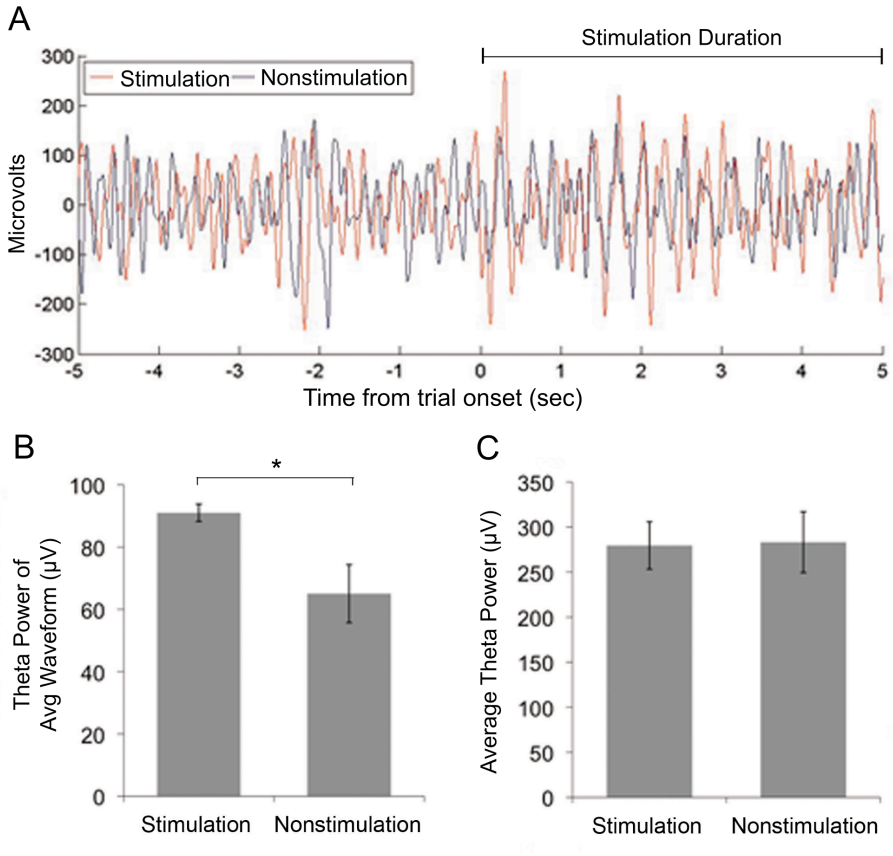

Figure 4. Hippocampal theta-phase resetting with stimulation. (A) An example subjects' final average waveform with electrical stimulation of the entorhinal region. Shown is an average of stimulation trials (red trace) and nonstimulation trials (blue trace) from one subject during spatial navigation. Time of zero is stimulation or nonstimulation trial onset; stimulation lasted 5 seconds. (B) Hippocampal theta-phase resetting averaged across four subjects during entorhinal stimulation and nonstimulation navigation trials. Shown is the theta power of the final waveform average (i.e. theta-phase resetting) for stimulation and nonstimulation post-trial onset (5-sec each). There was a significant increase in theta-phase resetting during stimulation vs. nonstimulation trials (*). (C) The average power of theta (microvolts [μV]) across individual trials did not differ between stimulation vs. nonstimulation periods (N = 4). This shows that there was similar power of the theta rhythm during individual stimulation and nonstimulation navigation trials. Error bars correspond to the standard error across subjects for each condition.

Subject demographics

Patient	Age	Gender	Handedness
1	40	M	R
2	28	M	R
3	20	F	R
4	46	F	R/L
5	52	F	R
6	35	M	R
7	27	M	R

Table 1. Subject demographics. Shown are the seven subjects age, gender and handedness.

Seizure foci and anti-seizure medications

Subject	REC	LEC	RAH	LAH	Seizure Focus	Anti-seizure Medication	Seizures
1	x				Left Medial Temporal	lamotrigine, oxcarbazepine	2 and 7 days prior
2	x			x	Extra-Temporal	lamotrigine, levetiracetam	2, 3, 4, 6, and 7 days prior
3	x		x		Left Medial Temporal	lacosamide	2 days prior
4		x	x		Left Medial Temporal	lacosamide, lamotrigine,	2 days prior
5			x	x	Supplementary Motor	levetiracetam, phenytoin, lacosamide	1, 2, 3, 4, and 5 days prior
6	x				Left Lateral Temporal	carbamazepine, lacosamide	1 and 2 days prior
7		x		x	Left Lateral Frontal	levetiracetam	1, 4, and 5 days prior

Table 2. Stimulated medial temporal lobe (MTL) regions, including right and left entorhinal region (REC, LEC) and right and left anterior hippocampal regions (RAH, LAH). Also shown are the clinically determined seizure-onset zones for each subject. Red indicates a stimulated region that fell within the seizure-onset zone for that subject. Days prior to stimulation when at least one seizure occurred and any anti-seizure medications that subjects were taking are also shown.

Electrode localizations

Patient	Region	Contact	MTL Localization	Brain Matter
1	REC	1	Entorhinal	white
		2	Entorhinal	white
2	REC	1	Entorhinal	white
		2	Entorhinal	white
	LAH	1	CA1	gray
		2	CA3DG	gray
3	REC	1	Entorhinal	white
		2	Entorhinal	gray
	RAH	1	CA1	gray
		2	ventricle	ventricle
4	LEC	1	Entorhinal	white
		2	Entorhinal	white
	RAH	1	CA1	gray
		2	CA1	gray
5	RAH	1	CA1	gray
		2	ventricle	ventricle
	LAH	1	CA1	gray
		2	CA1	gray
6	REC	1	Entorhinal	gray
		2	Perirhinal	gray
7	LEC	1	Entorhinal	white
		2	Perirhinal	gray
	LAH	1	CA1	gray
		2	CA1	white

Table 3. Subjects' electrode localizations. Region placements shown are for the two most distal electrode contacts from the right and left anterior hippocampus (RAH and LAH), and right and left entorhinal cortex (REC and LEC). Medial temporal lobe (MTL) electrodes were also localized to specific gray or white matter regions within the entorhinal region and hippocampal subregions CA1 or the combined region CA3 and dentate gyrus (CA3DG).

REFERENCES

1. Amaral, D.G. & Insausti, R. (1990) The hippocampal formation. The human nervous system, Academic Press, San Diego, 711–55
2. Augustinack JC, Helmer K, Huber KE, Kakunoori S, Zöllei L, Fischl B. (2010) Direct visualization of the perforant pathway in the human brain with ex vivo diffusion tensor imaging. Front Hum Neurosci. 4:42.
3. Duvernoy, H.M. (1998) The human hippocampus: Functional Anatomy, Vascularization, and Serial Sections with MRI, Springer, Berlin.
4. Ekstrom, A., Suthana, N.A., Salamon, N., Behnke, E., Bookheimer, S.Y., Fried, I. (2008) High-Resolution Depth Electrode Localization and Imaging in Patients with Pharmacologically Intractable Epilepsy. *Journal of Neurosurgery* 108, 812-5
5. Fried I, Wilson CL, Maidment NT, Engel J Jr, Behnke E, Fields TA, MacDonald KA, Morrow JW, Ackerson L. (1999) Cerebral microdialysis combined with single-neuron and electroencephalographic recording in neurosurgical patients. Technical note. J Neurosurg. (4):697-705.
6. Gumprecht HK, Widenka DC, Lumenta CB. (1999) BrainLab VectorVision Neuronavigation System: technology and clinical experiences in 131 cases. Neurosurgery 44:97-104;
7. Kahana MJ, Seelig D, Madsen JR. (2001) Theta returns. Curr Opin Neurobiol 11:739–44.
8. Schlaier JR, Warnat J, Dorenbeck U, Dorenbeck U Proescholdt M, Schebesch KM, et al. (2004) Image fusion of MR images and real-time ultrasonography: evaluation of fusion accuracy combining two commercial instruments, a neuronavigation system and a ultrasound system. Acta Neurochir (Wien) 146:271-6

9. Suthana NA, Ekstrom AD, Moshirvaziri S, Knowlton B, Bookheimer SY. (2009) Human hippocampal CA1 involvement during allocentric encoding of spatial information. Journal of Neuroscience 29:10512-9.

10. Yassa MA, Muftuler LT, Stark CE. (2010) Ultrahigh-resolution microstructural diffusion tensor imaging reveals perforant path degradation in aged humans in vivo. Proc Natl Acad Sci 107:12687-91.

11. Zeineh MM, Engel SA, Thompson P M, Bookheimer SY (2003) Dynamics of the hippocampus during encoding and retrieval of face-name pairs. Science 299:577-80.